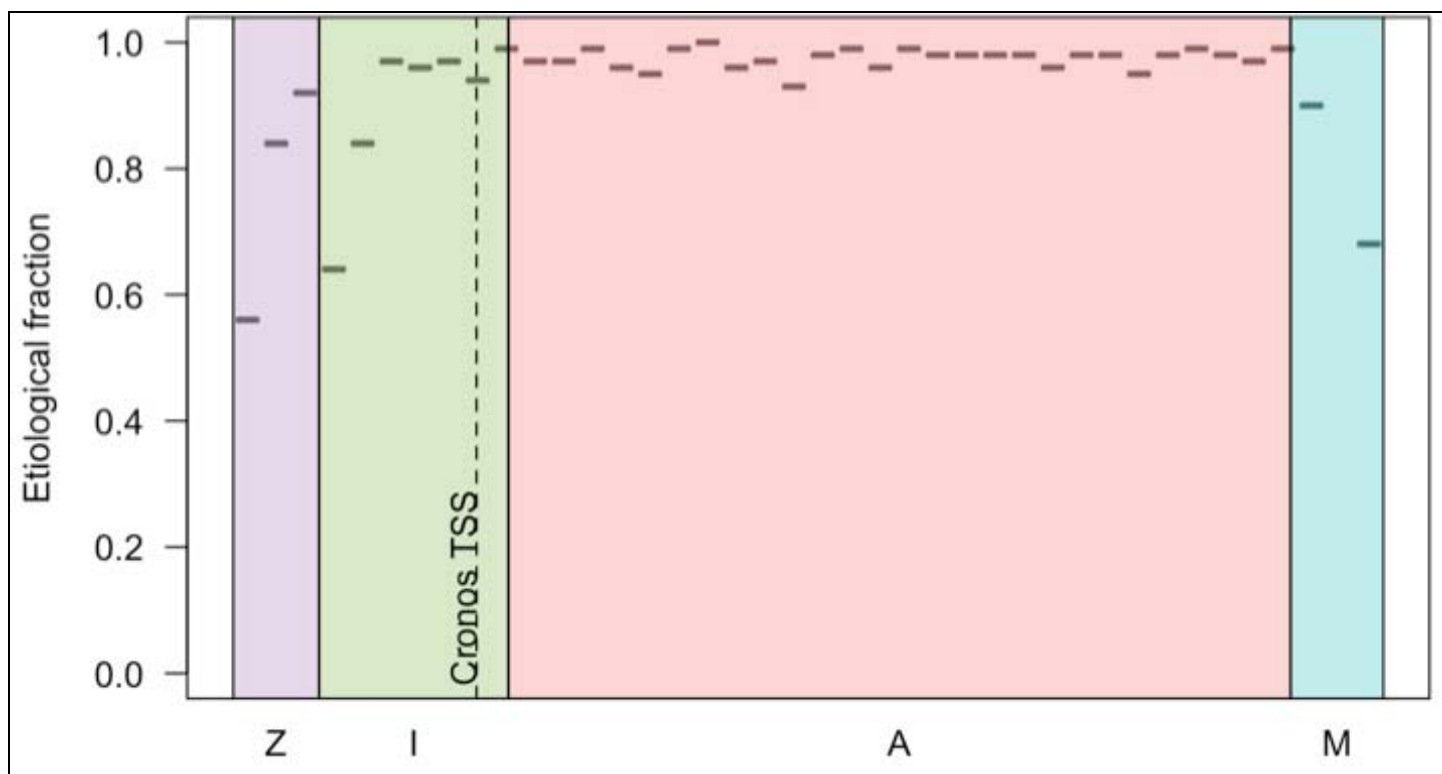


**Supplementary Figure 1**

Identification of an alternative, distal transcription start site in Titin.

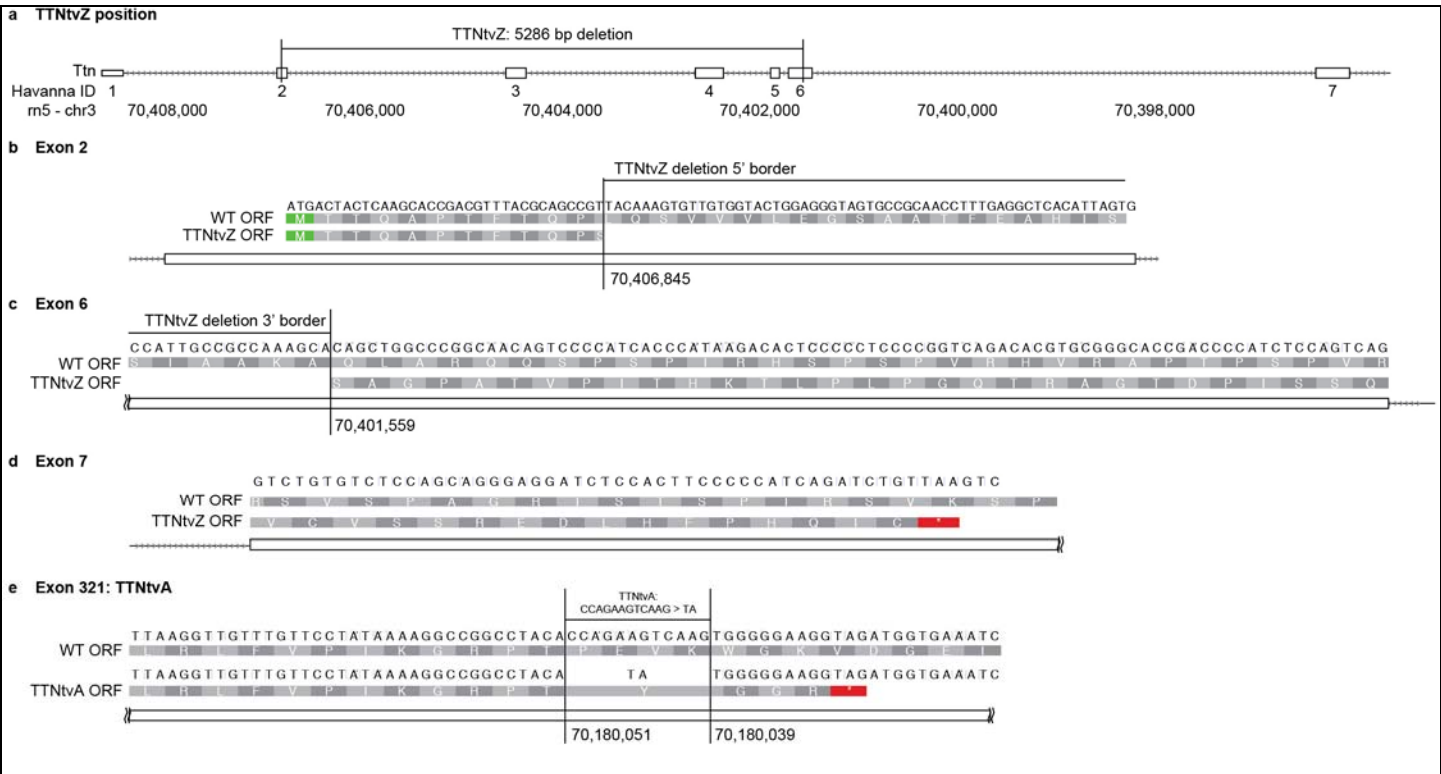
From the outside to inside; Track one shows the location of the subunits of Titin, the gene is on the antisense strand so is transcribed anti-clockwise in this view. Track two shows the gene structure of Titin with the exons shown as orange rectangles and introns by the black line. Track three shows the location of transcription start sites identified by the analysis of capped analysis of gene expression (CAGE) taken from human heart samples in the FANTOM5 consortium as identified using CAGEr. Track four shows the location of H3K4me3 ChIPSeq narrow peaks (a mark of active promoters) from fetal heart samples in the epigenome roadmap dataset. Track 5 shows HSK4me3 chip-Seq peaks from adult heart (left ventricle) taken from the epigenome roadmap dataset. Track 6 shows H3K9ac (also a mark of active promoters) taken from the fetal heart samples in the epigenome roadmap dataset. Together these data show that in the heart there are likely two transcription start sites, the canonical transcription start site at the beginning of the gene and another transcription start site found close to the start A-band, which appears to be most strongly utilised in the fetal heart but is still present in adult human heart.



## Supplementary Figure 2

Etiological fraction of TTNtv in 40 bins across the titin locus.

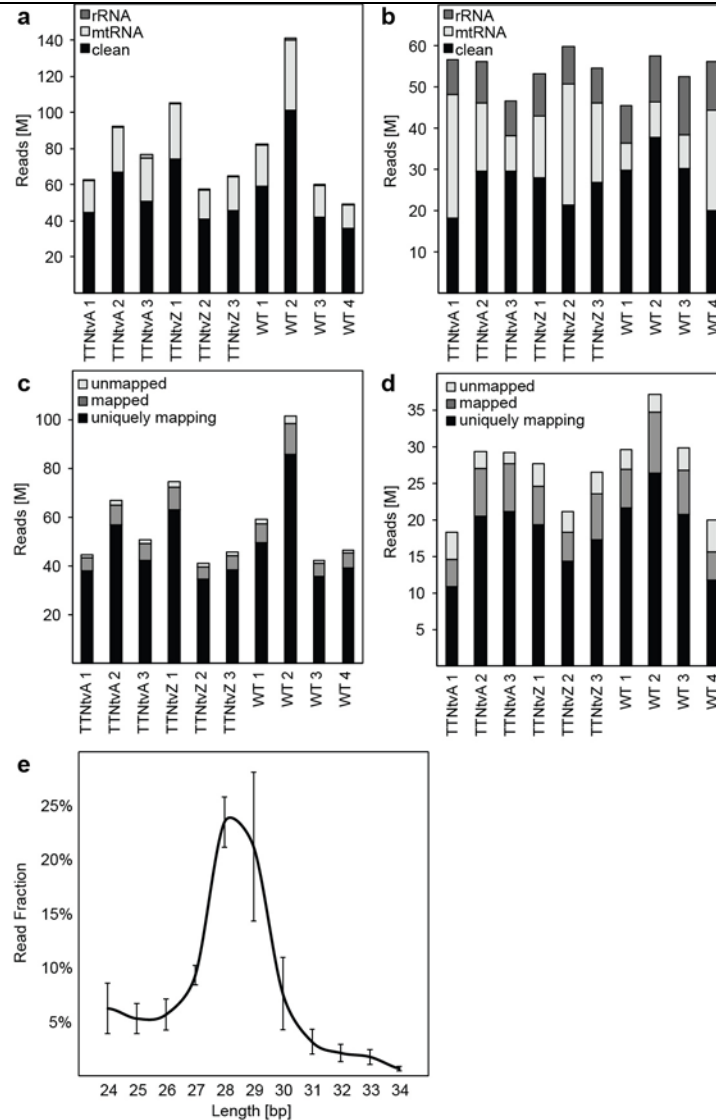
The constitutive (PSI >90%) regions of titin are split into 40 bins ranging from N- to C-terminus and the etiological fraction of TTNtv for each individual region are plotted. The dashed line marks the position of the internal *Cronos* promoter. Purple indicates Z-disc, green I-band, pink A-band and blue M-line.



**Supplementary Figure 3**

Truncating mutations introduced to F344 rats.

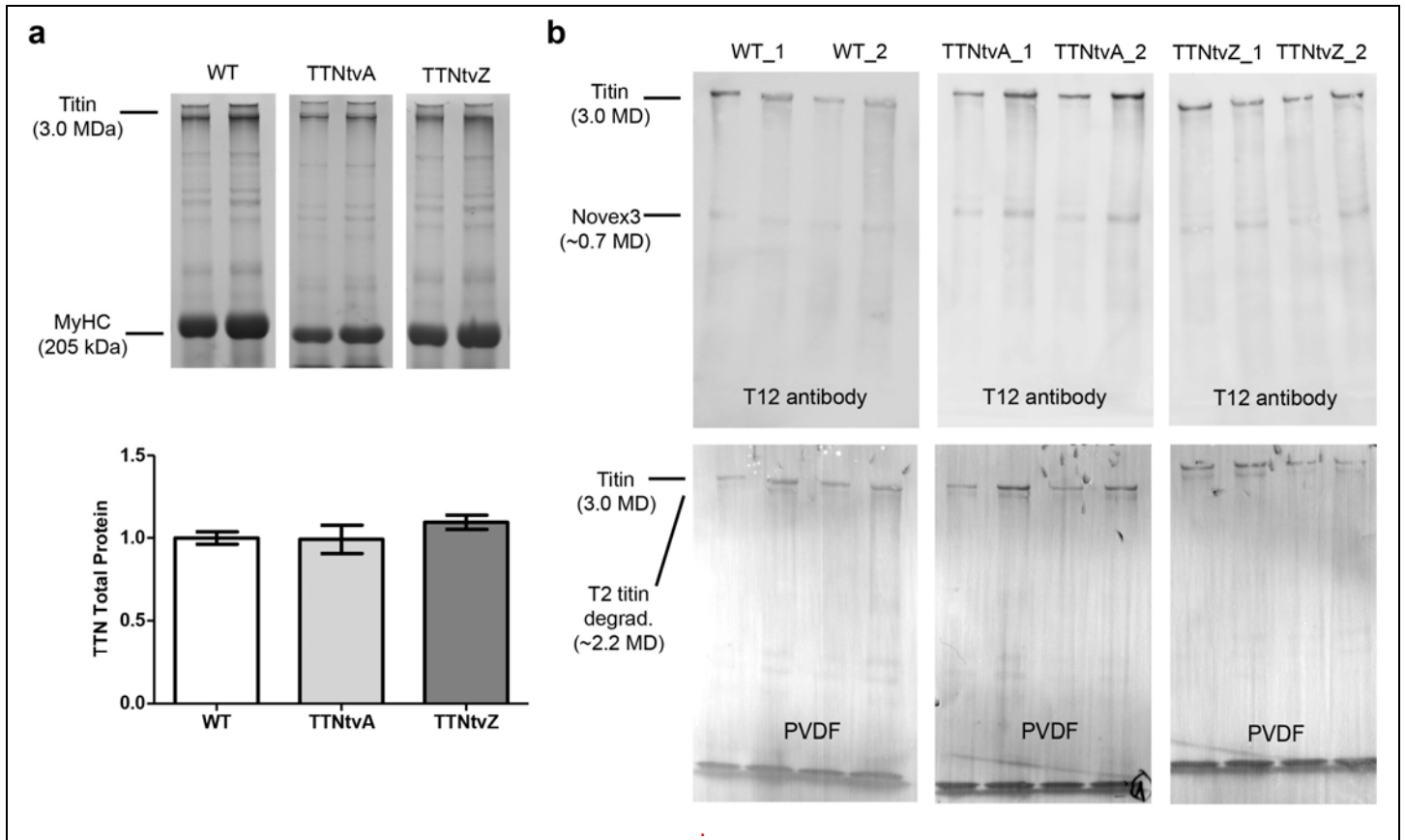
**a** The proximal truncating variant in titin is a large deletion located near the Z-disc at the N-terminus of the meta transcript (TTNtvZ). It spans from **b** exon 2 to **c** exon 6. Exons 3-5 are not present in TTNtvZ animals and can thus be used to assess transcription and translation from the WT allele in heterozygous animals. **d** The deletion causes a frameshift which results in a premature stop codon located in exon 7. **e** The truncating variant in the A-band is located in the large exon 312 and an indel that also causes a frameshift and introduces a stop codon shortly after.



**Supplementary Figure 4**

RNA sequencing and ribosome profiling data of TTNvA, TTNvZ and WT animals.

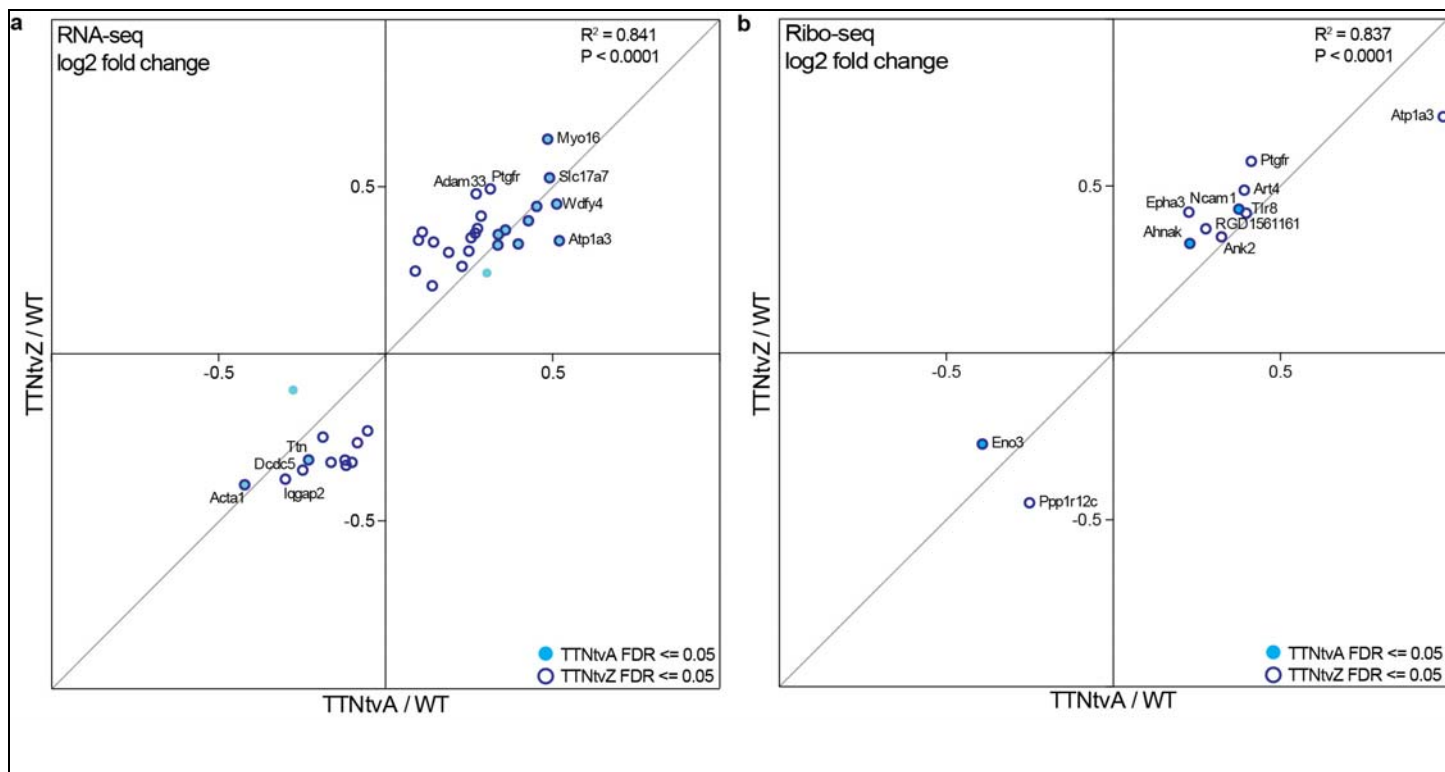
**a** RNA-seq reads and **b** Ribo-seq reads mapping to mitochondrial and ribosomal sequences were filtered out and the remaining sequences were mapped to the genome. Uniquely mapping **c** RNA-seq and **d** Ribo-seq reads were counted and used in later analyses to assess gene expression on the transcriptional and translational level. After adapter trimming, **e** Ribo-seq libraries displayed a size distribution typical for ribosome profiling experiments: Ribosome mostly protected RNA fragments with a size of 28 and 29 base pairs.



### Supplementary Figure 5

Absence of truncated ttn protein in TTNtvA and TTNtvZ rat hearts.

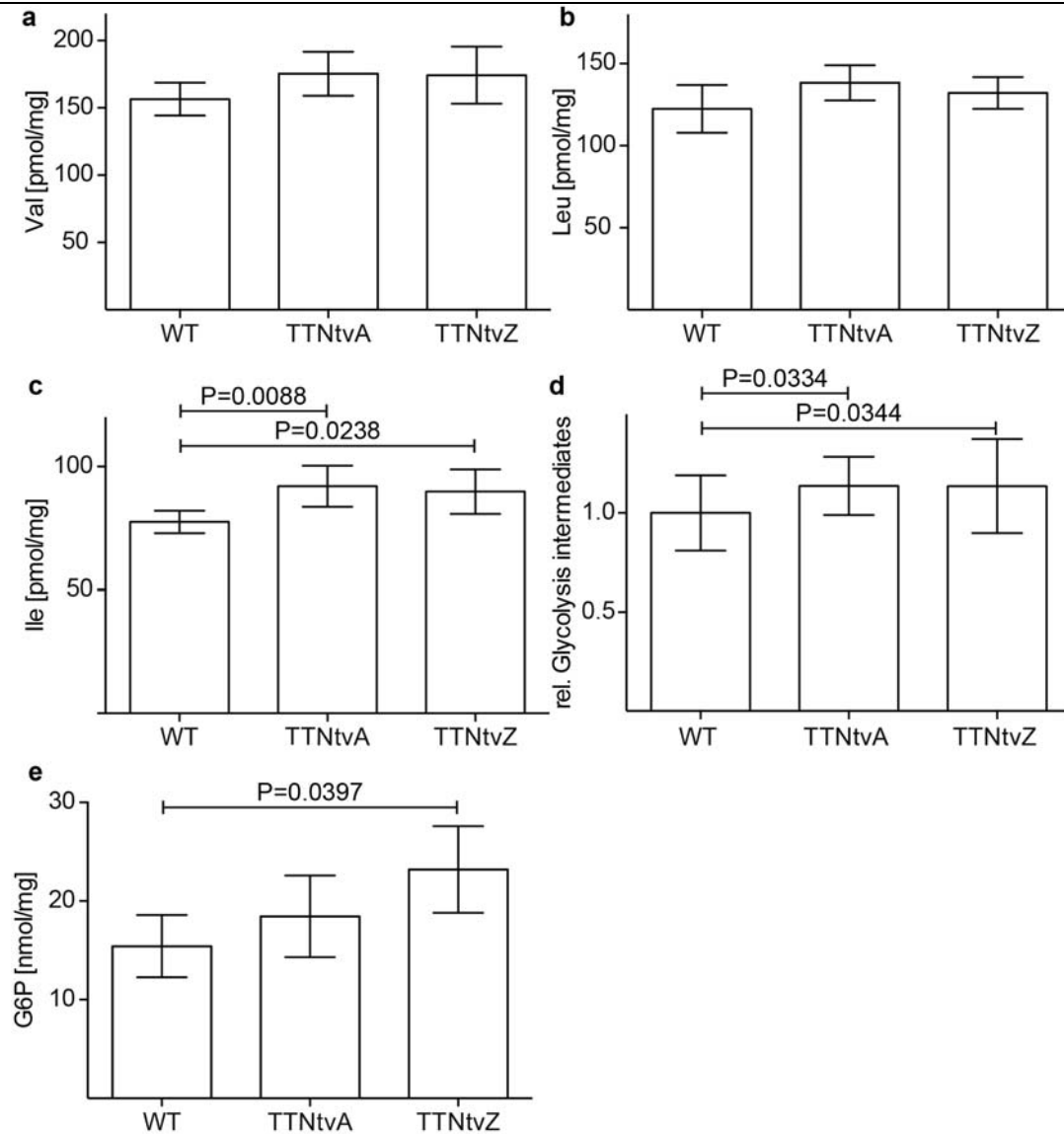
Representative titin gels and immunoblots of 3 month old WT, TTNtvA and TTNtvZ rat hearts. **a** SDS-PAGE (polyacrylamide gel electrophoresis) was performed on 2.5% polyacrylamide/1% agarose gels and total protein visualised by Coomassie Blue staining. Each sample was analyzed in duplicate at lower (left) and higher (right) protein concentrations respectively. Mhc was used as a loading control. Relative ratio of Ttn:Mhc was quantified (below) [Mean ± SEM] (n=4/group). **b** Immunoblotting analysis on 1.8% polyacrylamide/1% agarose gel transferred to PVDF and blotted with T12 antibody against titin and Novex3 (top panel). Corresponding PVDF blot was used as loading control (bottom panel).



### Supplementary Figure 6

Transcriptional and translational gene expression differences between WT and TTNtv animals.

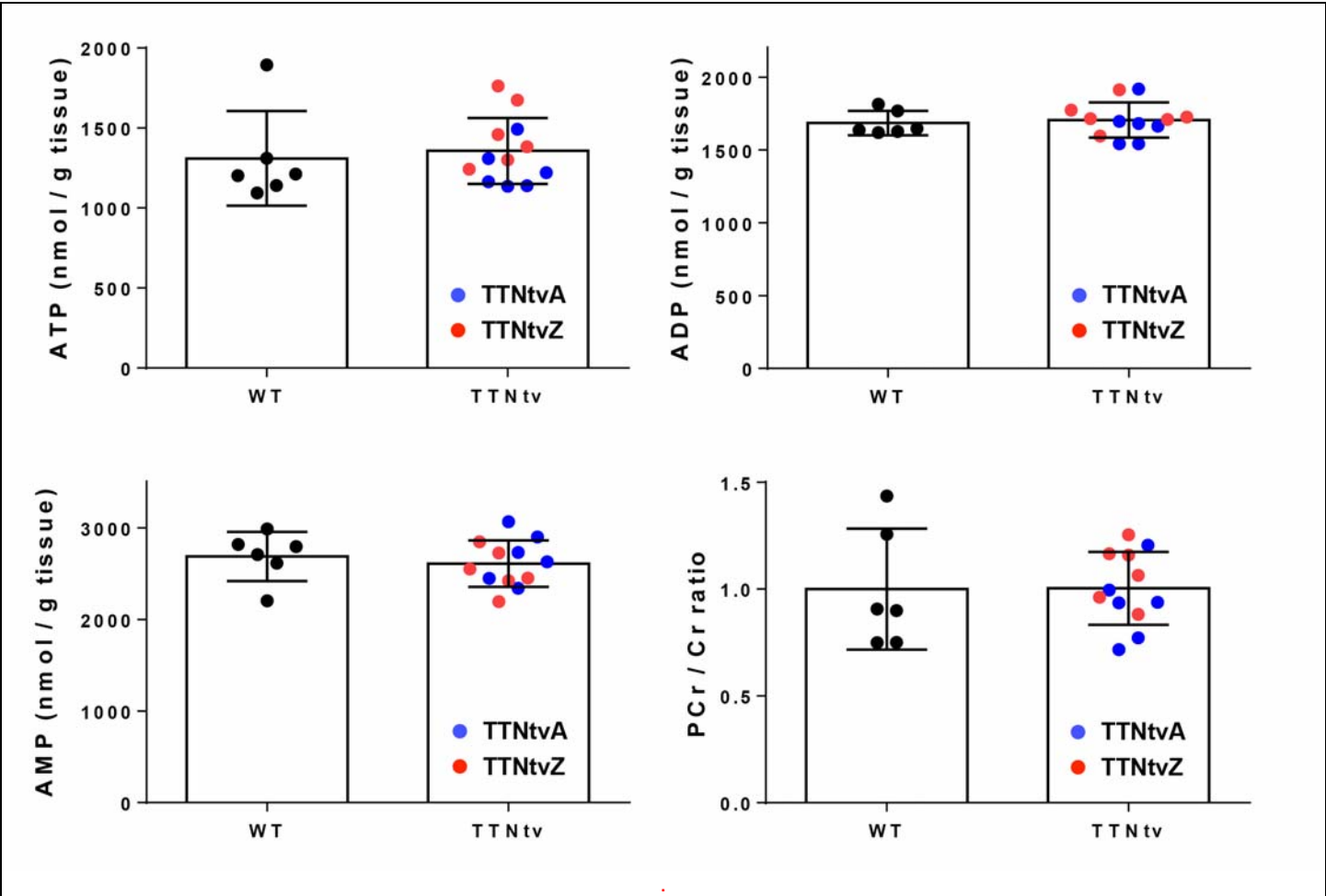
Differential gene transcription **a** and translation **b** is compared between TTNtv and WT animals. Both TTNtvA and TTNtvZ show highly correlated fold changes of differentially expressed genes (DEseq2 FDR  $\leq 0.05$ ) when compared to control animals (Pearson correlation). Genes that were not differentially expressed in any comparison were not considered.



### Supplementary Figure 7

Differences in cardiac metabolism between WT, TTNtvA and TTNtvZ animals.

Metabolite profiles showing branched chain amino acids (**a** valine, **b** leucine and **c** isoleucine), **d** sum of measured glycolytic intermediates (metabolites are detailed in **Table S3**) and **d** glucose-6-phosphate (G6P) in cardiac tissue of WT (n=6) and TTNtv (TTNtvA, n=6; TTNtvZ, n=6) rats. [Mean  $\pm$  SD, Dunnett].

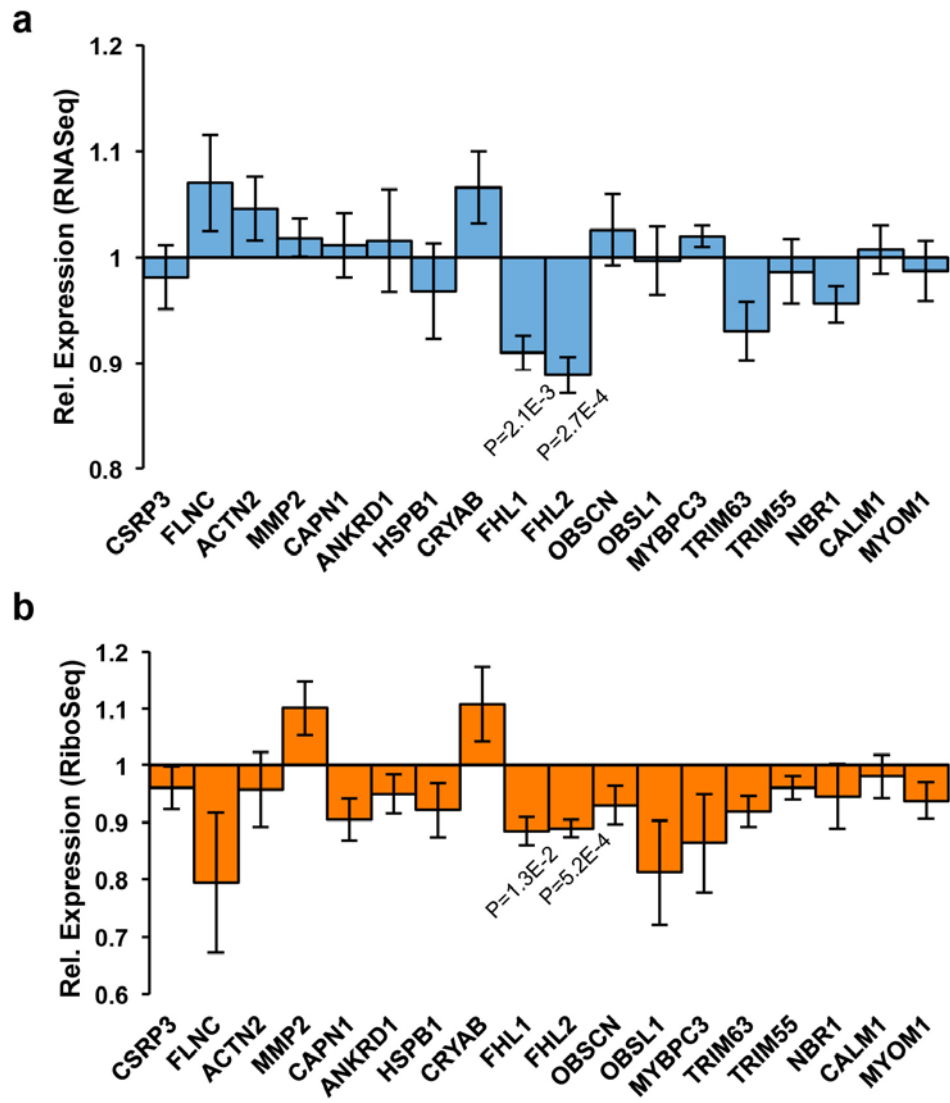


**Supplementary Figure 8**

TTNtv rat hearts have normal energy substrate abundance.

Metabolite levels of ATP, ADP, AMP and ratio of Phosphocreatine (PCr) versus Creatine (Cr) in 4 month old WT (n=6) and TTNtv (TTNtv-A, n=6; TTNtv-Z, n=6) rat hearts.

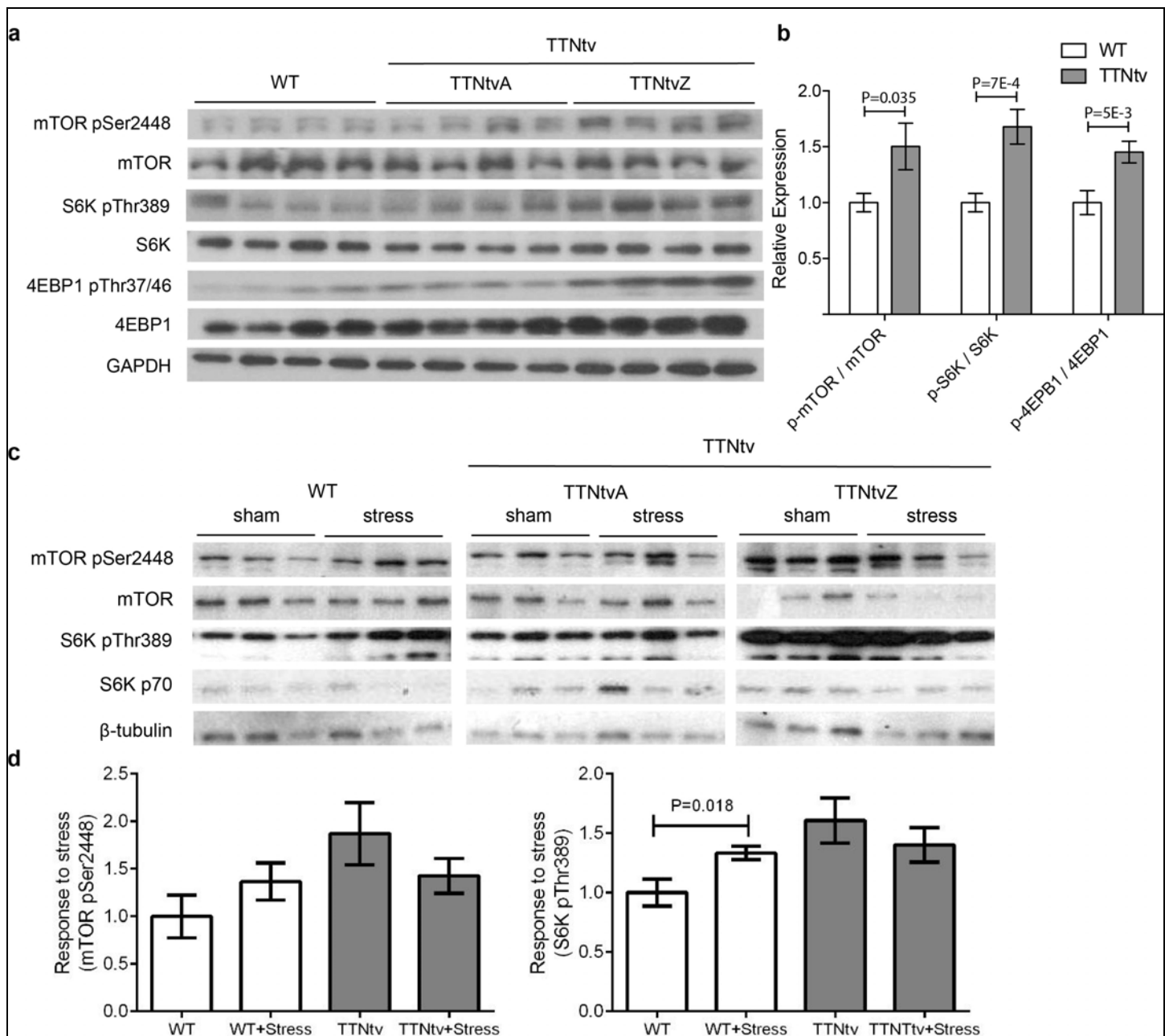




**Supplementary Figure 9**

Relative expression of titin-associated proteins in WT and TTNtv rats.

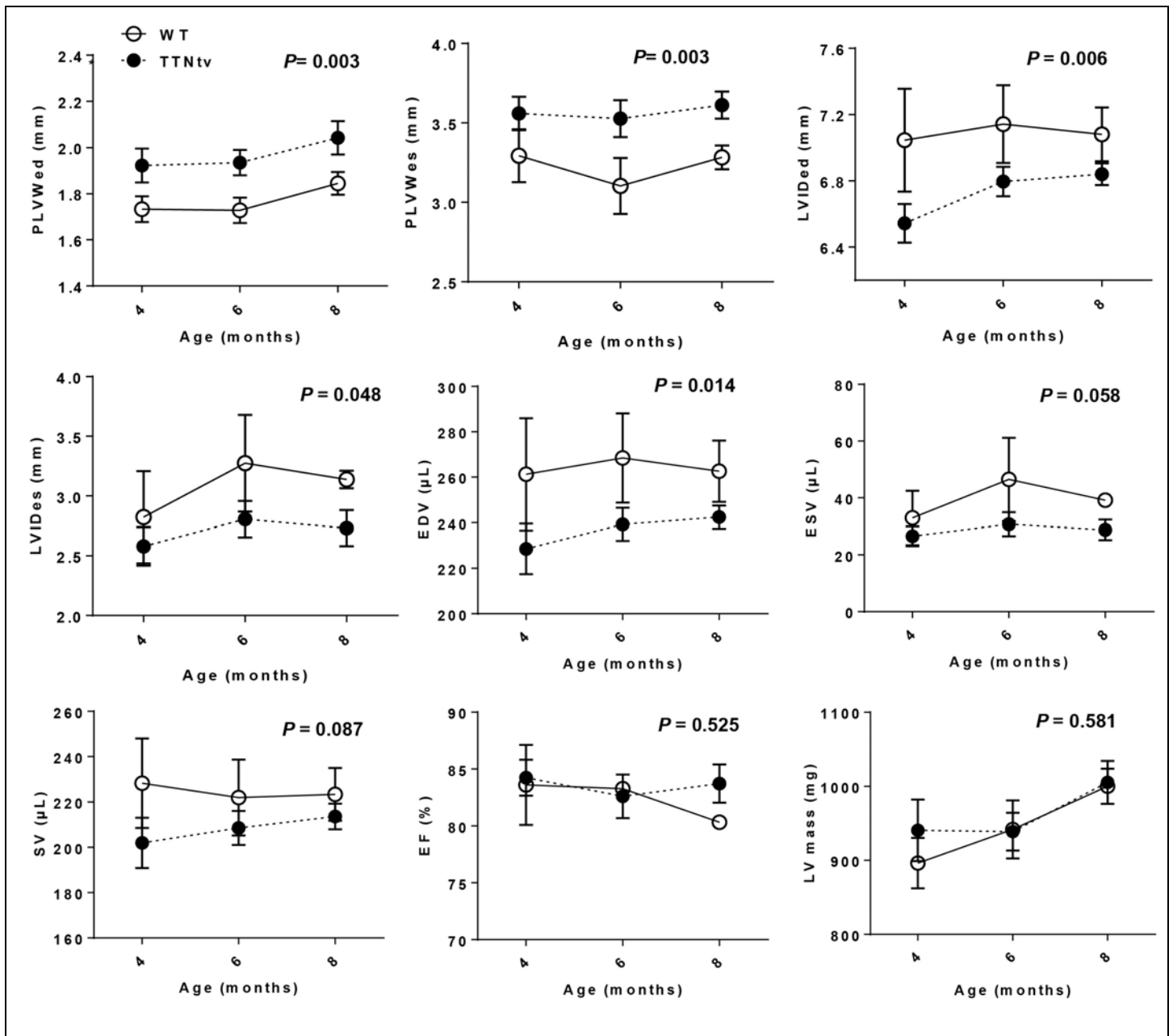
Relative difference (TTNtv / WT) in **a.** transcription and **b.** translation of titin-associated proteins showing significant decrease in FHL1 and FHL2 expression in 8 week old TTNtv (TTNtv-A, n=3; TTNtv-Z, n=3) as compared to WT (n=4) rats. Data shown are mean fold change  $\pm$  SEM. \*  $P < 0.05$  (Deseq2 P-value, not corrected for genome-wide testing).



**Supplementary Figure 10**

mTORC1 signalling is altered in TTNtv rat hearts.

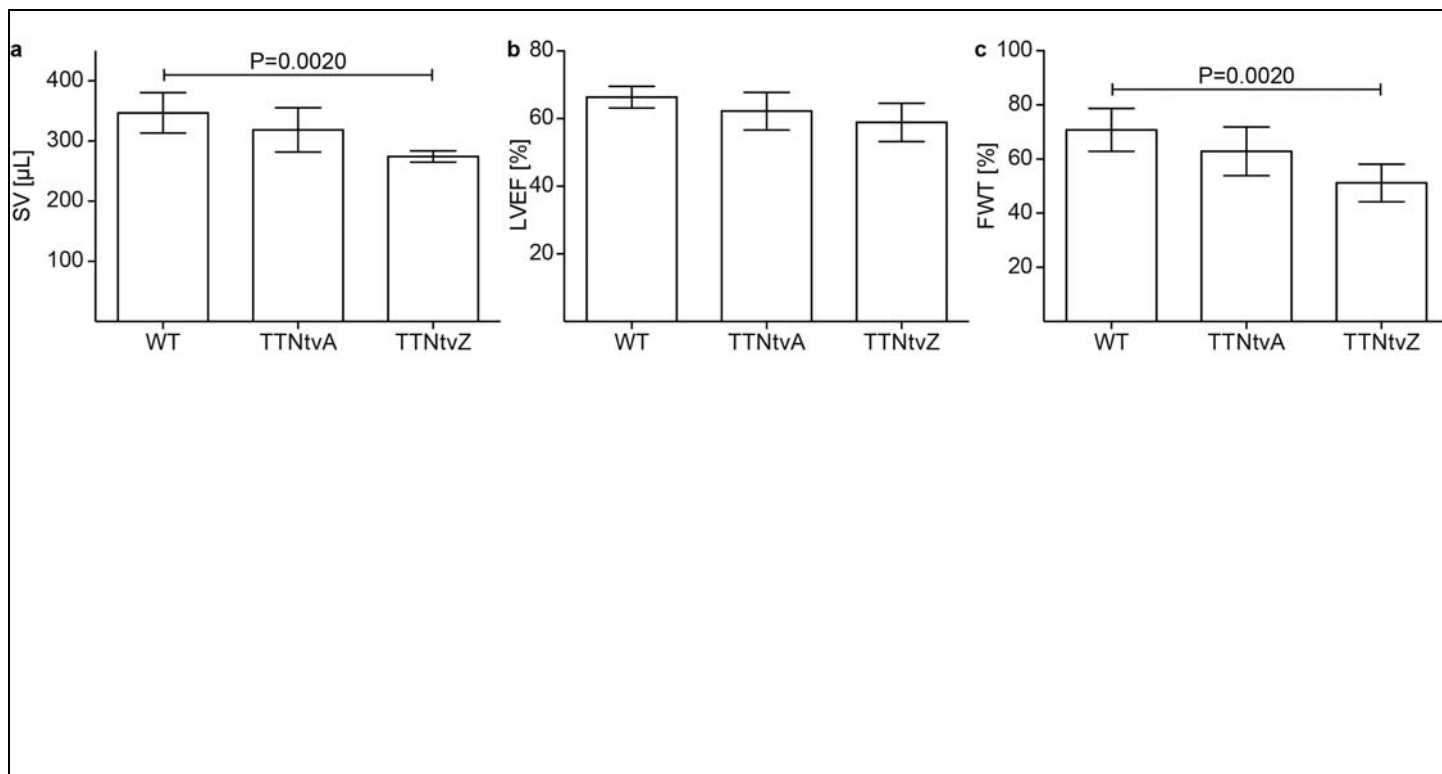
**a** Immunoblot analysis showing increased phosphorylation of mTOR (Ser2448), S6 kinase (Thr389) and 4EBP1 (Thr37/46) in TTNtv compared to WT hearts in hearts extracts from rats immediately post sacrifice. **b** Semi-quantitative densitometry of band intensities from several western blots across separate experiments and shown as [Mean  $\pm$  SEM, Students *t* test Welch correction] **c** Western blot analysis of phosphorylated mTOR (Ser2448) and S6 kinase (Thr389) in myocardial tissue following sham treatment or volume overload in WT and TTNtv rat hearts on the Langendorff apparatus perfused for the same duration. **d** Semi-quantitative densitometry representation of band intensities from blot in c and other experiments showing mTOR and S6K response to acute stress relative to WT unstressed hearts of the respective genotypes. [Mean  $\pm$  SD; versus unstressed WT hearts, Student's *t* test Students *t* test Welch correction].



**Supplementary Figure 11**

Young TTNtv rats display concentric remodelling.

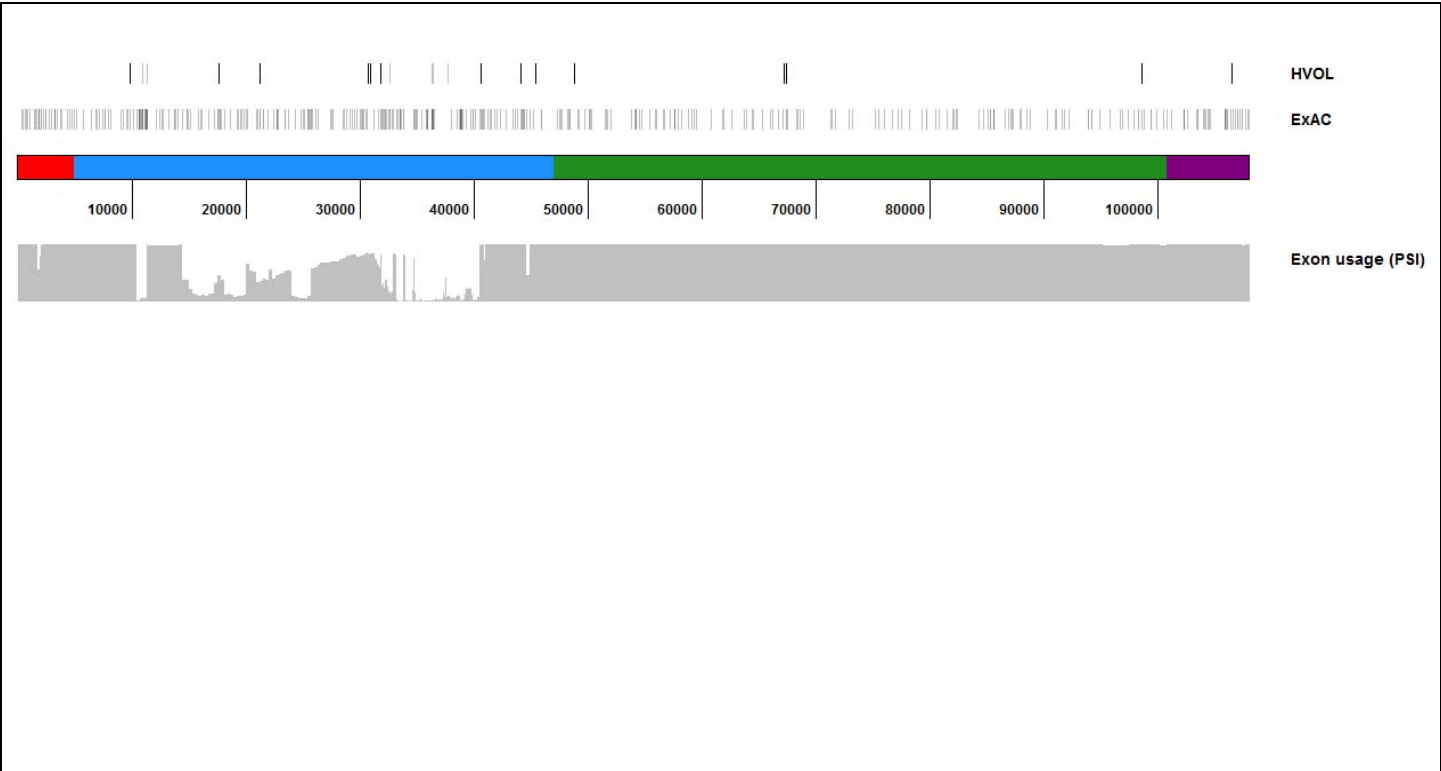
Echocardiographic measurements of 4 to 8 month old male WT (n=4) and TTNtv (TTNtvA n=4; TTNtvZ n=4) rats. PLVWed (mm), posterior left ventricular wall thickness end diastole; PLVWes (mm), posterior left ventricular wall thickness end diastole; LVIDed (mm), left ventricular internal diameter end diastole; LVIDes (mm), left ventricular internal diameter end systole; EDV (μL), end-diastolic volume; ESV (μL), end-systolic volume; SV (μL), stroke volume. EF (%), ejection fraction. P values indicate statistical analysis by two-way analysis of variance [ANOVA].



# Supplementary Figure 12

CMR in TTNtvA and TTNtvZ rats.

**a** SV (Stroke Volume), **b** LVEF (Left Ventricular Ejection Fraction) and **c** FWT (Fractional Wall Thickening) measured with CMR in 13-16 month old male WT (n=5) and TTNtv (TTNtvA, n=8; TTNtvZ, n=6) rats. [Mean  $\pm$  SD; Dunett].



**Supplementary Figure 13**

Distribution of TTNtv detected in the general population for MRI.

The top track shows the distribution of TTNtv in healthy volunteers (HVOL) who were phenotyped using cardiac magnetic resonance imaging. The track below depicts the distribution of TTNtv from the ExAC data. Only truncations located in exons with PSI > 15% are shown.